REPORT

OPTICS

Breaking Lorentz reciprocity to overcome the time-bandwidth limit in physics and engineering

K. L. Tsakmakidis,[1]*†‡ L. Shen,[2]* S. A. Schulz,[1]§ X. Zheng,[3] J. Upham,[1] X. Deng,[2] H. Altug,[4] A. F. Vakakis,[5] R. W. Boyd[1,6]‡

A century-old tenet in physics and engineering asserts that any type of system, having bandwidth $\Delta\omega$, can interact with a wave over only a constrained time period Δt inversely proportional to the bandwidth ($\Delta t \cdot \Delta\omega \sim 2\pi$). This law severely limits the generic capabilities of all types of resonant and wave-guiding systems in photonics, cavity quantum electrodynamics and optomechanics, acoustics, continuum mechanics, and atomic and optical physics but is thought to be completely fundamental, arising from basic Fourier reciprocity. We propose that this "fundamental" limit can be overcome in systems where Lorentz reciprocity is broken. As a system becomes more asymmetric in its transport properties, the degree to which the limit can be surpassed becomes greater. By way of example, we theoretically demonstrate how, in an astutely designed magnetized semiconductor heterostructure, the above limit can be exceeded by orders of magnitude by using realistic material parameters. Our findings revise prevailing paradigms for linear, time-invariant resonant systems, challenging the doctrine that high-quality resonances must invariably be narrowband and providing the possibility of developing devices with unprecedentedly high time-bandwidth performance.

More than 100 years ago, K. S. Johnson introduced the concept of the now-ubiquitous quality factor (Q factor) to characterize the sharpness of a resonance (*1*, *2*). In that work, a practical way to characterize the quality of a resonant system was introduced by defining a unitless number $Q = \omega_0/\Gamma$, where ω_0 is the system's resonance frequency and Γ the decay rate of the wave energy (*1*, *2*). Since then, it has been understood that the higher the Q factor of a resonant system, the narrower its bandwidth—higher Qs lead to sharper resonances (*1*).

This notion, that high-quality (high-Q) resonances must invariably be narrowband, has not been challenged since Johnson's original work and pervades an extremely broad range of resonant and wave-guiding systems in physics and engineering (Fig. 1). Its justification arises from basic Fourier-reciprocity considerations (*3*–*5*): Inside any linear, passive (lossy and time-invariant) resonant system, e.g., in a cavity micro- or nanoresonator, the excited-wave amplitude $\alpha(t)$ will decay as $\alpha(t) \propto \cos(\omega_0 t) \times e^{-(1/2)\Gamma t}$, where Γ can be due to nonradiative (inelastic or dephasing) and/or radiative processes (coupling to the continuum of the surrounding medium). Hence, in the resonance approximation and in the usual underdamped regime ($\Gamma/2 << \omega_0$) (*3*, *4*), the intensity I in the frequency domain will be given by

$$I(\omega) \propto |\alpha(\omega)|^2 \propto \frac{\left(\frac{\Gamma}{2}\right)^2}{(\omega-\omega_0)^2 + \left(\frac{\Gamma}{2}\right)^2} \qquad (1)$$

from which it is immediately seen that $\Delta\omega$ around ω_0 is $\Delta\omega = (\omega_0 + \Gamma/2) - (\omega_0 - \Gamma/2) = \Gamma$. Thus, by definition, the bandwidth of the resonant system is the loss rate Γ. Any attempt to reduce the overall losses and, hence, store the wave for an increased time $\Delta\tau$ will automatically decrease $\Delta\omega$—a limitation that arises from simple time-harmonic considerations.

We show that this "fundamental" time-bandwidth limit characterizing resonant devices can be overcome by breaking Lorentz reciprocity, i.e., by conceiving (asymmetric) systems whose responses change when the source and the receiver are interchanged

$$\iiint_V \mathbf{J}_1\mathbf{E}_2\,dV \neq \iiint_V \mathbf{J}_2\mathbf{E}_1\,dV \qquad (2)$$

where $\mathbf{J}_1$ and $\mathbf{J}_2$ are two sources within a volume V generating the electric fields $\mathbf{E}_1$ and $\mathbf{E}_2$, respectively. Specifically, we introduce and analyze a realistic system that exceeds the time-bandwidth limit anticipated by the system's Q factor by orders of magnitude.

The time-bandwidth limitation is a completely general phenomenon, characterizing the storage capacity of all linear, time-invariant resonant and wave-guiding devices, from photonics to acoustics, cavity quantum electrodynamics and optomechanics, and atomic and molecular physics, as well as mechanical and structural systems (Fig. 1). It should not be confused with the mathematical time-bandwidth limit $\sigma_t^2\sigma_\Omega^2 \geq 1/4$, where σ_t^2 is the time variance of a signal $x(t) \in L_2(\Re)$ and σ_Ω^2 its frequency variance, i.e., with the uncertainty principle characterizing Fourier-integral pairs in signal analysis and communications (*6*) and which, among others, only has a lower bound. Although both limits often bear the same name, the time-bandwidth limit in physics and engineering characterizes the storage capacity of the devices themselves, not the mathematical Fourier properties of the respective signals. In addition to resonant physical devices outlined above, the physical time-bandwidth limit described in this study also arises in guiding structures, such as slow-light wave guides or bulk media (e.g., electromagnetically induced transparency in ultracold atomic gases) (*7*–*12*). Here, a number of works have shown that any such passive structure can support slow waves over a finite bandwidth $\Delta\omega$ inversely proportional to the group index n_g. Hence, a structure of fixed length L cannot delay a wave packet of bandwidth larger than $\Delta\omega$ by more than a time $\Delta\tau \sim n_g L/c$, where c is the speed of light in vacuum. In other words, the "delay-bandwidth product" $\Delta\tau \cdot \Delta\omega$, characterizing a linear, time-invariant slow-wave structure, has an upper limit C (*13*–*15*). This threshold is quite stringent: Depending on the specifics of the particular slow-wave structure, it can vary between $C \sim 10$ and 100, to within an order of magnitude (*7*–*10*, *13*–*15*), and cannot be broken by means of a nonlinear or gain mechanism, such as stimulated Raman or stimulated Brillouin scattering, because such fundamental effects as gain saturation, group-velocity, and attenuation dispersions make $\Delta\tau$ inversely proportional to a power of $\Delta\omega$—e.g., $\Delta\tau \sim \Delta\omega^{-\alpha}$, $\alpha = 2$ or 3 (*7*, *9*, *14*)—an even stricter limitation. A further adverse consequence of the time-bandwidth limit in physics and engineering is that it constrains the response time of the above devices because the higher the Q factor of a system (i.e., the narrower the bandwidth), the longer it takes to respond to an external signal. However, a high Q factor is a prerequisite for high sensitivity (*16*). Thus, short response times and high sensitivity tend to counteract each other, and a compromise has to be found between the two. A well-known manifestation of this limitation concerns microfabricated quartz tuning forks, currently the most successful and widespread method for shear-force detection. With a Q factor at ambient conditions of the order of 10^3 to 10^4—necessary for probing interaction forces less than ~200 pN—the response time of a tuning fork, $\tau = 2\sqrt{3}Q/\omega_0$, is limited to being greater than ~300 ms (*16*), i.e., the scanning speeds are slow.

[1]Department of Physics, University of Ottawa, 25 Templeton Street, Ottawa, ON K1N 6N5, Canada. [2]Institute of Space Science and Technology, Nanchang University, Nanchang 330031, China. [3]State Key Laboratory of Modern Optical Instrumentation, Zhejiang University, Hangzhou 310027, China. [4]Bioengineering Department, École Polytechnique Fédérale de Lausanne (EPFL), 1015 Lausanne, Switzerland. [5]Department of Mechanical Science and Engineering, University of Illinois at Urbana-Champaign, 1206 West Green Street, Urbana, IL 61801, USA. [6]Institute of Optics and Department of Physics and Astronomy, University of Rochester, Rochester, NY 14627, USA.
*These authors contributed equally to this work. †Present address: Bioengineering Department, EPFL, 1015 Lausanne, Switzerland.
‡Corresponding author. Email: kostsakmakidis@gmail.com (K.L.T.); rboyd@uottawa.ca (R.W.B.). §Present address: Centre for Advanced Photonics and Process Analysis, Cork Institute of Technology, and Tyndall National Institute, Cork, Ireland.

To overcome the time-bandwidth limit by breaking Lorentz reciprocity, consider a wave s_+ impinging (either from a surrounding uniform medium or from a guiding structure) on a reciprocal system and exciting a mode of amplitude α inside it (Fig. 2A). The key idea is that although the basic Fourier-transform reciprocal relations do, in general, remain valid, they can be applied separately at the input and output ports of a system if it is asymmetric (nonreciprocal) in its transport properties, i.e., if Lorentz reciprocity is broken. The equation describing the time evolution of $\alpha(t)$ is (*17*)

$$\frac{d\alpha}{dt} = i\omega_0\alpha - \left(\frac{1}{\tau_0} + \frac{1}{\tau_{out}}\right)\alpha + \rho_{in}s_+ \qquad (3)$$

where $1/\tau_0$ and $1/\tau_{out}$ are, respectively, the internal (owing, e.g., to dissipative losses) and outcoupling (owing, e.g., to radiative loss to the surrounding medium) decay rates, and ρ_{in} is the rate of in-coupling of energy from the s_+ wave to the resonant system. Here, following the standard convention of temporal coupled-mode theory, we assume that $|s_+|^2$ is normalized to the incident power, whereas $|\alpha|^2$ is normalized to the incident energy (i.e., the units of $|s_+|$ are $\sqrt{2W/s}$) (*17*). The rate of in-coupling of energy into the resonant system ρ_{in} is proportional to the $\Delta\omega$ of the system ($\pi\rho_{in} \leftrightarrow \Delta\omega$) (*17*, *18*) [see also (*19*)], whereas the lifetime $\Delta\tau$ of the excited mode is, as shown from Eq. 3, $\Delta\tau = 1/(1/\tau_0 + 1/\tau_{out}) \approx \tau_{out}$ because we normally operate in the overcoupled (underdamped) regime where the rate of energy escape from (and energy coupled into) the excited resonant system is greater than the rate of internal dissipation, $2/\tau_{out} >> 2/\tau_0$. The key point is that, because of time-reversal symmetry, it can be shown rigorously that the in-coupling rate ρ_{in} is always tied to the out-coupling rate ρ_{out} through the exact relation (in units of $|\alpha|$) (*17*):

$$|\rho_{in}| = \frac{2}{\tau_{out}} \qquad (4)$$

Thus, the product between the system's bandwidth and the wave-system interaction time (lifetime) $\Delta\tau$ is always, for reciprocal systems, of the order of $\Delta\omega\Delta\tau \leftrightarrow \pi|\rho_{in}|\tau_{out} \sim 2\pi$, i.e., we recover the aforesaid physical time-bandwidth limitation, in which $\Delta\omega$ and $\Delta\tau$ characterizing a resonant or guiding device are reciprocally related. However, if Lorentz reciprocity is by some means broken in this passive, linear, and time-invariant resonant system, $|\rho_{in}|$ and τ_{out} can become completely decoupled, in which case the product $\Delta\omega\Delta\tau$ (or, equivalently, $|\rho_{in}|\tau_{out}$) can be engineered at will and take on arbitrarily large values—i.e., in such a case we can exceed the conventional time-bandwidth limit by an arbitrarily large factor.

Consider a heterostructure made of a dielectric layer (silicon, Si) bounded asymmetrically by a gyroelectric semiconductor (indium antimonide, InSb) on the bottom and a metal layer (silver, Ag) on the top (Fig. 2B). Lorentz reciprocity in this linear, passive, and time-invariant system can be broken by applying a static magnetic field B_0 in the $-y$ direction (*20*–*22*), causing a precession of the electron magnetic dipole moments in the semiconductor with a frequency $\omega_c = eB_0/m*$ (where e and m^* are the charge and effective mass of the electrons, respectively). A small ac magnetic field propagating along the heterostructure also causes a precession of the semiconductor electrons' dipole moments around the B_0 ($-y$) axis at the frequency of the ac field. The interaction of the ac field with the semiconductor is thus, overall, captured by the following asymmetric permittivity tensor (*23*)

$$\varepsilon = \varepsilon_0\varepsilon_\infty \begin{bmatrix} \varepsilon_1(B_0) & 0 & i\varepsilon_2(B_0) \\ 0 & \varepsilon_3 & 0 \\ -i\varepsilon_2(B_0) & 0 & \varepsilon_1(B_0) \end{bmatrix} \qquad (5)$$

where $\varepsilon_1 = 1 - (\omega + i\nu)\omega_p{}^2/\{\omega[(\omega + i\nu)^2 - \omega_c{}^2]\}$; $\varepsilon_2 = \omega_c\omega_p{}^2/\{\omega[(\omega + i\nu)^2 - \omega_c{}^2]\}$; $\varepsilon_3 = 1 - \omega_p{}^2/[\omega(\omega + i\nu)]$, with the plasma frequency of InSb taken to be $\omega_p = 4\pi \times 10^{12}$ rad/s ($f_p = 1/T_p = 2$ THz); $\varepsilon_\infty = 15.6$; $\omega_c = 0.2\omega_p$; and $B_0 = 0.2$ T [where ε, permittivity; v, the (permittivity) loss factor; p, plasma; T, (time) period]. For the other two layers, we take $\varepsilon_{Si} = 11.68$ and $\varepsilon_{Ag} = 1 - \omega_{pe}{}^2/[\omega(\omega + i\omega_\tau)]$, with $\omega_{pe} = 1.367 \times 10^{16}$ rad/s and $\omega_\tau = 2.733 \times 10^{13}$ rad/s (*20*, *21*, *23*). Because of the application of the external magnetic bias, the heterostructure supports one-way edge (magnetoplasmon) modes, robust against surface imperfections and roughness, whose dispersion relation is governed by (*20*, *21*, *23*)

$$\tanh(\alpha_d d) = -\frac{\alpha_s + \frac{\varepsilon_2}{\varepsilon_1}k + \frac{\varepsilon_V\alpha_m}{\varepsilon_m}}{\left(\alpha_s + \frac{\varepsilon_2}{\varepsilon_1}k\right)\frac{\varepsilon_r\alpha_m}{\varepsilon_m\alpha_r} + \frac{\varepsilon_V\alpha_d}{\varepsilon_r}} \qquad (6)$$

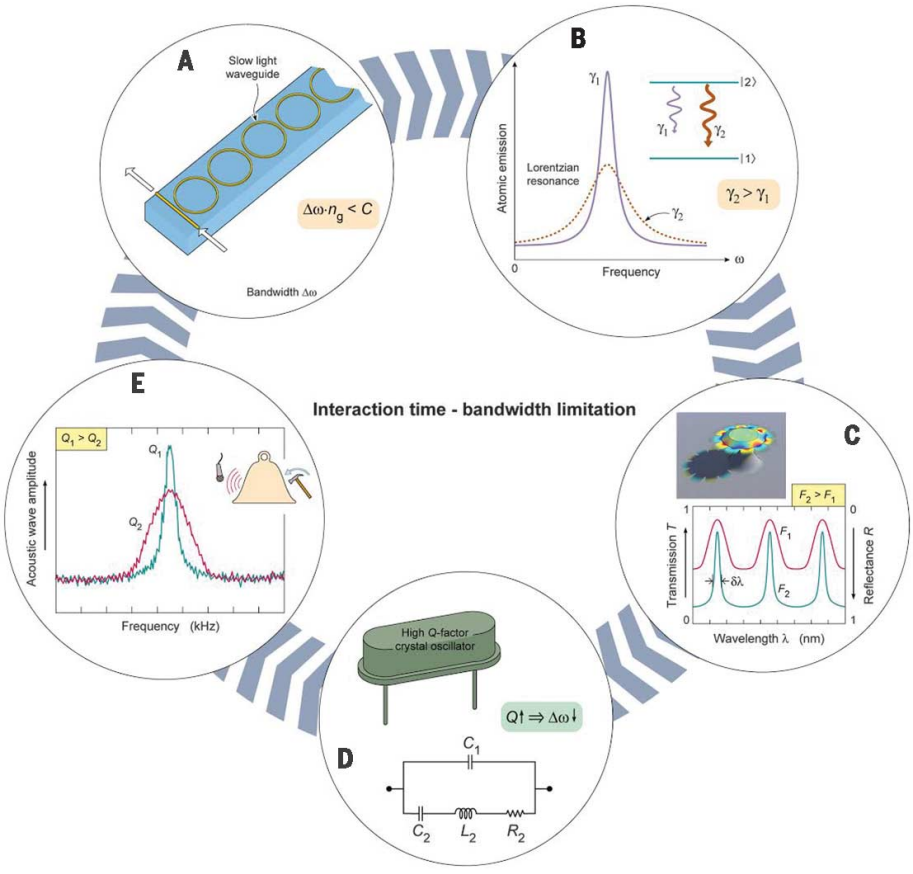

Fig. 1. The "fundamental" time-bandwidth limit, in various forms, in reciprocal systems in physics and engineering. (**A**) In all types of slow-light wave guides, the attained delays Δt are inversely proportional to the guide's bandwidth, $\Delta\omega$ ($\Delta t \propto \Delta\omega^{-1}$) or, even more severely, to a power of it (e.g., $\Delta t \propto \Delta\omega^{-\alpha}$, $\alpha = 2$ or 3) (*7*–*15*). (**B**) In atomic and molecular physics, the linewidth γ of an atomic transition is inversely proportional to the decay rate arising from dephasing and inelastic or spontaneous-emission processes (*3*). Likewise, the time required to perform the transformation $|\Psi_i> \rightarrow |\Psi_f> = e^{-iHt}|\Psi_i>$, where $|\Psi_i>$ and $|\Psi_f>$ are two orthogonal states and H is the (time-independent) Hamiltonian, is $\tau_{tr} \sim |(E_f - E_i)/\hbar|^{-1}$, where E_f and E_i are the corresponding eigenvalues of H (*24*). (**C**) In all types of (dielectric or plasmonic) cavity resonators, higher finesses F result in narrower resonance bandwidths (*3*–*5*, *16*–*18*). (**D**) In crystal (quartz) oscillators; piezoelectric, micro-/nanomechanical, or elastic systems; and energy-harvesting devices, the response times are directly proportional to the system's Q factor, $\tau_{rsp} \propto Q$. Higher Q factors lead to enhanced sensitivities but also to larger response times (*16*). (**E**) In acoustic devices and systems, such as in ultrasound, elastic-wave, or wave-modulation spectroscopies, increased quality factors give rise to narrower spectral responses.

where $\alpha_d = \sqrt{k^2 - \varepsilon_r k_0^2}$; $k_0 = \omega/c$ is the vacuum wave number; $\varepsilon_r = \varepsilon_{Si}$ and $d = 0.08\lambda_p (\lambda_p = 2\pi c/\omega_p)$ are the relative permittivity and thickness of the Si layer, respectively; $\alpha_s = \sqrt{k^2 - \varepsilon_V k_0^2}$; $\varepsilon_V = \varepsilon_\infty(\varepsilon_1 - \varepsilon_2^2/\varepsilon_1)$ is the Voigt permittivity; and $\alpha_m = \sqrt{k^2 t - \varepsilon_m k_0^2}$, where ε_m is the relative permittivity of Ag.

Upon solving Eq. 6, we plot in Fig. 2C the band structure of this type of surface state, showing clearly that the band diagram is asymmetric with respect to the wave vector $-k$ axis, giving rise to a frequency region where no backward-propagating ($k < 0$) states exist (breaking of Lorentz reciprocity). For a carefully designed structure, that region can be made to be below the continuous band(s) of the bulk modes in the semiconductor and above the band associated with surface states at the semiconductor-metal interface. Thus, in that frequency region, complete unidirectional propagation (CUP) is rigorously attained: An excited edge state can propagate strictly only in the forward (positive z, k) direction and cannot be back-reflected or couple either to bulk modes in the semiconductor or to semiconductor-metal surface states. The two frequencies, ω_{CUP}^- and ω_{CUP}^+, bounding the CUP region (see Fig. 2C) can be identified analytically from Eq. 6 by letting $|k| \to \infty$ [see (*19*)]

$$\omega_{CUP}^{\pm} = \frac{1}{2}\left(\sqrt{\omega_c^2 + 4\omega_p^2 \frac{\varepsilon_\infty}{\varepsilon_\infty + \varepsilon_r}} \pm \omega_c\right) \quad (7)$$

from which we see that the bandwidth of the CUP region is simply $BW_{CUP} = \omega_c (= eB_0/m*)$.

Figure 3A illustrates successive snapshots from full-wave simulations of the propagation of a pulse, whose bandwidth is within the CUP region, along the heterostructure shown in Fig. 2B. The structure is terminated in the z direction by the Ag cladding (which also covers the end of the heterostructure), creating an impenetrable barrier for the pulse along z. Because in that frequency region there are no surface modes allowed at the Ag-InSb interface and the pulse cannot scatter to bulk modes inside InSb or to backward modes in the $-z$ direction (see Fig. 2C), the pulse eventually localizes near the Si-Ag interface, where it decays with time until it is completely absorbed (right-hand graph of Fig. 3A). As seen in Fig. 3A, initially, at t = 15 ps (= $30T_p$), the pulse broadens (because of dispersion) to a longitudinal length of $d_i^l \cong 215.5$ μm [and a transverse size of $d_i^T \cong 12.1$ μm; see also fig. S1, A and B, (*19*)], but when it reaches the rightmost end, it gives rise to a strongly localized plasmonic resonance. At t = 50 ps (= $100T_p$), the pulse is spatially compressed to a deep-subwavelength spot of $d_f^l \cong 0.165$ μm (and $d_f^T \cong 0.02$ μm), i.e., it is spatially squeezed by a factor of ~0.79×10^6 in two dimensions, while its peak intensity is enhanced by a factor of ~10^3 [see also fig. S1, D and E, (*19*)] (where T, transverse; p, period; l, length in the longitudinal direction; i, initial; f, final). The localized field thus behaves exactly as if it were confined inside a subwavelength, "zero-dimensional" (*24*) cavity resonator perfectly matched to the incident-wave medium: It is confined in a specified region of space—where it was in-coupled without reflections, decaying with time inside (but not propagating within or escaping from) this region—and with the field amplitude being dramatically enhanced inside this zero-dimensional cavity. Figure 3B further shows that the so-trapped field can be released on demand by reversing the direction of the external magnetic bias B_0 (B_0 = 0.2 T → B_0 = −0.2 T) at any point while the field is localized.

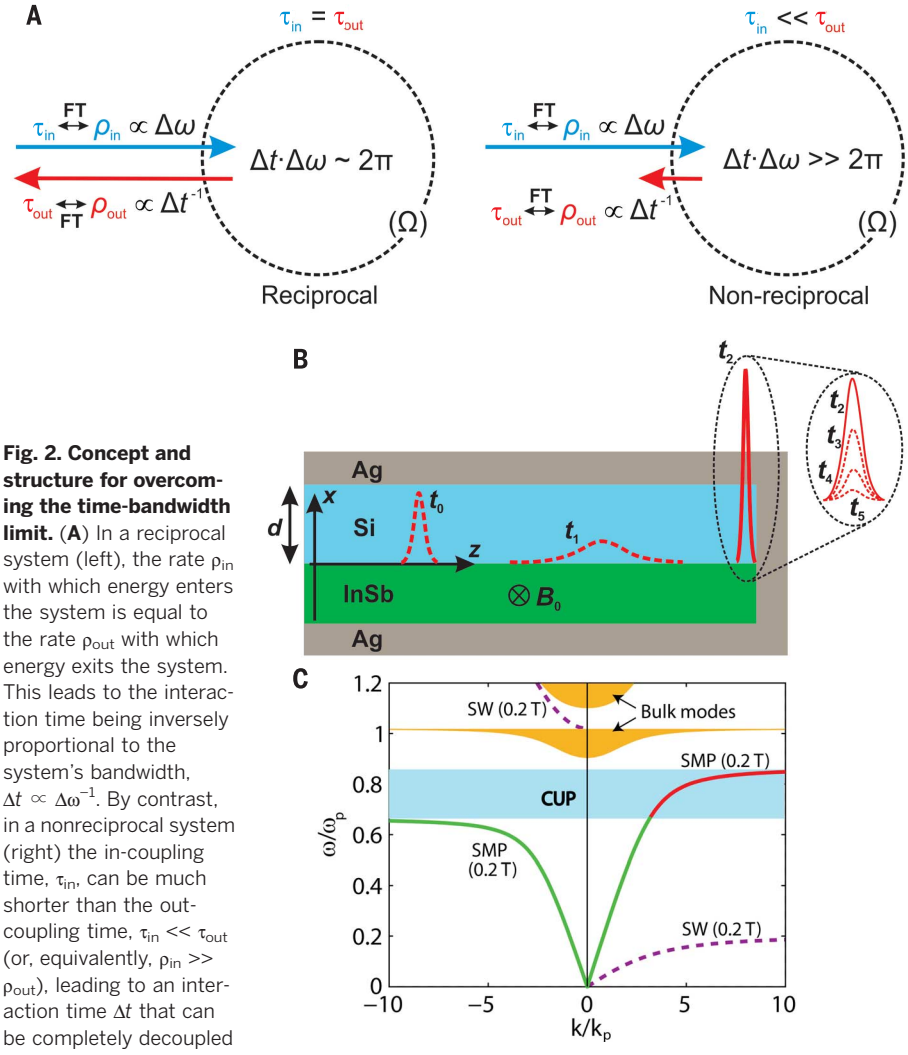

Fig. 2. Concept and structure for overcoming the time-bandwidth limit. (**A**) In a reciprocal system (left), the rate ρ_{in} with which energy enters the system is equal to the rate ρ_{out} with which energy exits the system. This leads to the interaction time being inversely proportional to the system's bandwidth, $\Delta t \propto \Delta\omega^{-1}$. By contrast, in a nonreciprocal system (right) the in-coupling time, τ_{in}, can be much shorter than the out-coupling time, $\tau_{in} << \tau_{out}$ (or, equivalently, $\rho_{in} >> \rho_{out}$), leading to an interaction time Δt that can be completely decoupled from the bandwidth $\Delta\omega$. Consequently, the product $\Delta t \cdot \Delta\omega$ can now take on arbitrarily large values—much larger than the standard 2π limit. In both cases, the Fourier-transform reciprocity, relating τ_{in} (τ_{out}) to ρ_{in} (ρ_{out}) and to $\Delta\omega$ (Δt^{-1}), is always valid, but is applied separately to the input and the output of the system. (**B**) Schematic illustration of the nonreciprocal configuration used for breaking the time-bandwidth limit. It consists of a Si layer sitting on top of a gyroelectric semiconductor, InSb. The two layers are bounded by Ag on three sides. The external, static magnetic field B_0 is applied in the $-y$ direction. A pulsed magnetic-current source excites a surface magnetoplasmon, which propagates unidirectionally, without back-scattering or back-reflections, from left to right, all the way until the rightmost Si-Ag interface where it is spatially compressed, greatly enhanced in amplitude, and robustly localized (compare to Fig. 3A). There are no propagating states allowed in the $-z$ direction, inside InSb, or along the InSb-Ag interface [see also (C)]. Once localized at the rightmost end, a pulse can only decay with time owing to dissipative losses, exactly as if it were confined inside a passive, zero-dimensional (*24*) cavity resonator (right inset). (**C**) Band diagram of the structure of (B) for the case where the external magnetic field is applied in the $-y$ direction (B_0 = 0.2 T). Shown are, for both positive and negative longitudinal wave vectors k, the dispersion curve of the herein studied surface magnetoplasmons (SMPs), the surface wave at the InSb-Ag interface (SW), and the region of the bulk modes in InSb. The area shaded in blue indicates the band region where CUP of the considered surface magnetoplasmon is attained. The part of the SMP dispersion curve inside that region is indicated in red.

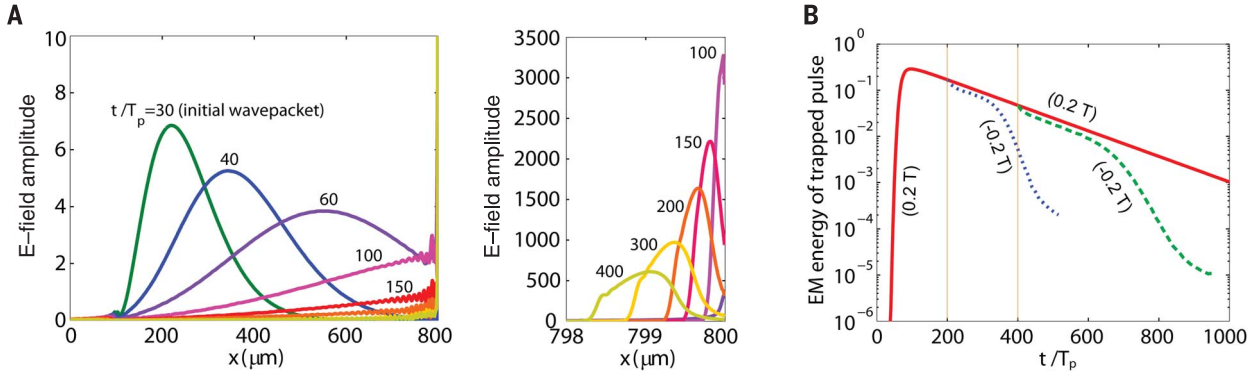

Fig. 3. Open-cavity localization and overcoming the "fundamental" delay-time–bandwidth limit. (**A**) One-dimensional snapshots of the propagation of a pulse of central frequency 1.5 THz and bandwidth 0.2 THz, exciting a one-way surface magnetoplasmon in the heterostructure of Fig. 2B, at successive time instants. Shown on the right are close-up views around the localization region at the rightmost end of the heterostructure of Fig. 2B. Note the change in the scale of the vertical axis and the dramatic ensuing field enhancement upon entering that zero-dimensional open-cavity region. E-field, electric field. (**B**) Electromagnetic energy as a function of time in an imaginary box surrounding the pulse's localization region. When the external static magnetic field B_0 = 0.2 T is constantly in the $-y$ direction, the energy of the localized pulse inside the box simply decays with time (red curve) owing to dissipative losses, as expected [and as shown in (A)]. By contrast, when the direction of the B_0 field is suddenly reversed (B_0 = −0.2 T), the pulse may now escape in the backward ($-z$) direction (compare to Fig. 2C), as a result of which the wave energy inside the box rapidly diminishes. Two examples of this are shown here, one at t = 200T_p (blue dotted line) and another at t = 400T_p (green dashed line), demonstrating storage times of up to ~400T_p.

A somewhat reminiscent light-trapping, storage, and releasing scheme also exists, e.g., for ultraslow and stored light in atomic electromagnetically induced transparency (EIT) (*8*, *11*, *12*) but with the fundamental difference being that therein the bandwidth is narrow (*25*) and/or the attained storage times are inversely proportional to the bandwidth (or to a power of it) (*7*, *9*, *13*–*15*). Figure S2 (*19*) shows how in this linear, time-invariant system the whole broad spectrum of the pulse is progressively stored in its trapping region.

Because of the above Lorentz reciprocity–breaking characteristics, the rates of in-coupling (ρ_{in}) and out-coupling (ρ_{out}) of energy in this open cavity are not equal: Whereas ρ_{in} is proportional to the system's in-coupling bandwidth ($\rho_{in} \propto \Delta\omega_{in}$), the out-coupling rate tends to zero ($\rho_{out} = 1/\tau_{out} \rightarrow 0$) because the light wave cannot radiatively escape from the region it is confined in. Thus, on the basis of our previous analysis, we expect that in this system the interaction time $\Delta\tau = 1/(1/\tau_0 + 1/\tau_{out}) \approx \tau_0$ and the resonant bandwidth $\Delta\omega$ should be completely decoupled, not inversely proportional as in all conventional (reciprocal) resonant and waveguiding systems. In other words, we expect that our system can be extremely broadband even in the limit of ultrahigh Q factors where the total losses may tend to zero and the storage times to infinity ($\Delta\tau \rightarrow \infty$).

To demonstrate that $\Delta\tau$ and $\Delta\omega$ are independent of one another, Fig. 4 summarizes the results of successive full-wave simulations for the cases where (i) the loss rate ν is progressively increased, but B_0 remains constant and (ii) B_0 progressively increases, but ν remains constant. We see from Fig. 4, A and B, that while ν is increased, the total optical losses of the system also progressively increase as expected, but the bandwidth of the effective cavity remains constant in all cases, $\Delta\omega \approx 2.5$ THz, unaffected by the gradually increased loss rate. Even in the case where an extremely low-loss InSb film ($\nu/\omega_p = 10^{-4}$) with realistic material parameters is used [e.g., electron density $N_e = 1.1 \times 10^{16}$ cm^{-3}; see (*26*) and (*19*)], we find that whereas the energy decay rate Γ is ~10^9 s^{-1} and therefore the bandwidth $\Delta\omega$ should conventionally be anticipated to be small, ~10^{-3} THz ($\Delta\omega = \Gamma$, see discussion immediately after Eq. 1), the actual bandwidth of the nonreciprocal zero-dimensional cavity at the rightmost end of our structure is still large and ~2.5 THz—more than three orders of magnitude above the fundamental time-bandwidth limit of reciprocal (linear and passive) systems. Furthermore, we find that the pulse is seamlessly incoupled to the localization point (whereas for any reciprocal, lossless resonant system, the in-coupling time would have tended to infinity for progressively smaller losses), where it is rigorously confined (Fig. 3A and leftmost parts of Fig. 4, A and B). Thus, the performance of this system, both in terms of bandwidth and response time, exceeds that of any standard reciprocal system (*4*, *5*, *16*–*18*, *23*, *24*) by orders of magnitude.

For case (ii), where the external static magnetic field B_0 progressively increases, Fig. 4, C and D, shows that the bandwidth of the zero-dimensional cavity increases accordingly (by 100%), as expected from Eq. 7, but the optical losses (and hence the storage times) remain approximately constant, increased only by ~5%—unaffected by the bandwidth increase. The small increase in the total optical losses that we observed in our simulations for this latter case is because the slope of the band (i.e., the pulse's group velocity) reduces with increasing B_0, leading to higher overall optical losses (*27*). We see from Fig. 4, C and D, that, in this case too, the nonreciprocal cavity is above the fundamental time-bandwidth limit of conventional (reciprocal) resonant systems by more than two orders of magnitude. The results presented in Fig. 4, therefore, convincingly show that in this system, the interaction time (lifetime) $\Delta\tau$ and the bandwidth $\Delta\omega$ are independent and decoupled of one another, owing to the breaking of Lorentz reciprocity ($\rho_{in} >> \rho_{out}$), giving rise to an, in principle, unlimited time-bandwidth performance—i.e., to breaking of the Q-factor limit in the sense that $\Delta\tau$ and $\Delta\omega$ are not inversely proportional to one another anymore [although Fourier uncertainty (*6*) is still obeyed when considered separately at the input and output ports, as shown in Fig. 2A and discussed above].

Finally, in existing, reciprocal ultraslow- and stored-light configurations (e.g., those exploiting dark states in EIT or in coherent population trapping), the storage time is fundamentally inversely proportional to the system's bandwidth or to a power of it (*7*–*15*). In contrast, in the present nonreciprocal scheme, the storage time is solely determined by the loss rate (which, as shown in Fig. 4, is decoupled from the bandwidth) and/or the time until which we switch off the external magnetic field, releasing the localized pulse (Fig. 3B). Because both of these parameters (loss rate and duration of B_0 being "on") are, here, completely independent of the system's bandwidth, the attained delay-bandwidth products can now, in principle, become arbitrarily large. For instance, Fig. 3B demonstrates storage times of up to ~400T_p for a pulse of bandwidth 0.2 THz, whereas conventionally, for reciprocal-guiding structures, the anticipated maximum

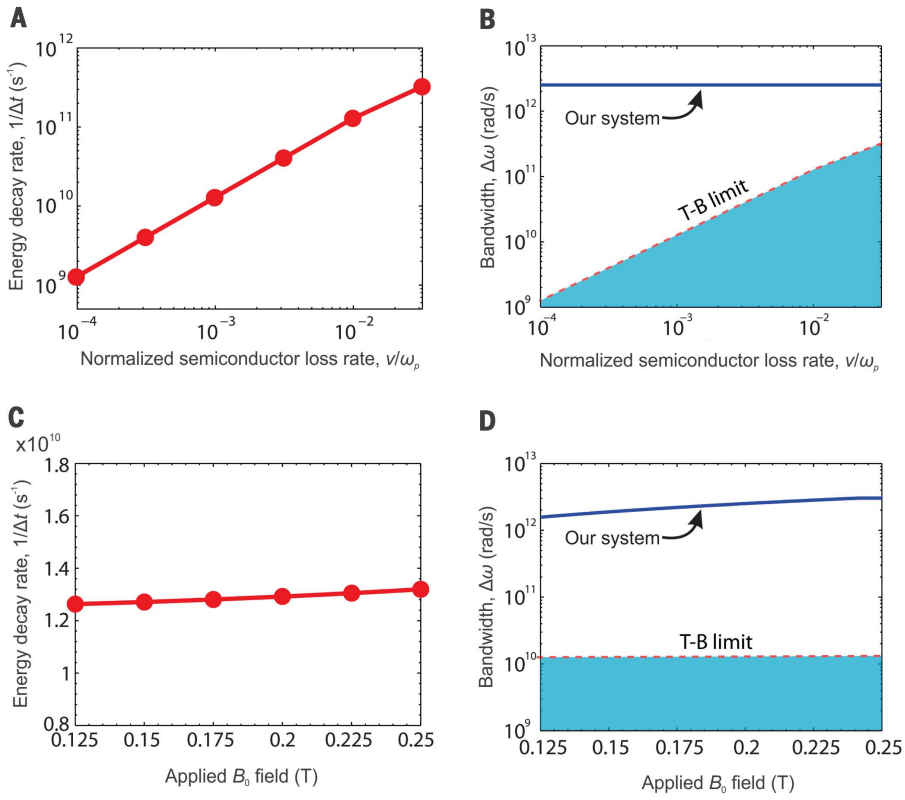

Fig. 4. Decoupling of interaction time and bandwidth and overcoming the Fourier-reciprocity ($\Delta\omega \sim \Delta t^{-1}$) limit. (**A**) and (**B**) For increasing scattering losses v in the semiconductor, the decay rate of the localized pulse's energy progressively increases (A), signifying reduced interaction (storage) times, as expected, whereas in all cases the bandwidth $\Delta\omega$ of the one-way effective cavity remains constant (B) (blue line). The energy decay rate sets the fundamental bandwidth limit [$\Delta\omega = \Gamma \sim \Delta t^{-1}$, time-bandwidth (T-B) limit] characterizing conventional, reciprocal systems and which is here broken by more than three orders of magnitude, as shown in (B). By contrast, for increasing values of the static magnetic bias B_0, the energy decay rate remains approximately constant (**C**), whereas the bandwidth of the zero-dimensional open cavity progressively increases (**D**) (blue line) [see also fig. S3B for further clarity (*19*)]. Note from (D) that in this case, the bandwidth of the zero-dimensional cavity is more than two orders of magnitude above the fundamental time-bandwidth limit of reciprocal resonant devices—i.e., larger than the energy decay rate by more than two orders of magnitude. All the results shown here have been obtained from full-wave and analytic calculations, as detailed in (*19*). In both (B) and (D), the dashed red lines are the solid red lines shown in (A) and (C), respectively.

delay and storage times would be (*7*–*15*) $\Delta t_{max} \sim (\Delta\omega)^{-1}$ or less, i.e., $\Delta t_{max} \sim 5$ ps $= 10T_p$. Thus, our nonreciprocal device is above the conventional delay time–bandwidth limit of state-of-the-art slow-light systems by more than a factor of 40.

The consequences of our findings carry over to all resonant and wave-guiding systems in physics and engineering where the above time-bandwidth limit appears in disguise, including subdiffraction imaging systems (where there is always a trade-off between spatial and temporal resolution) (*28*) and broadband invisibility cloak devices (where there is a trade-off between scattering reduction and broadband operation) (*29*, *30*). On a more basic level, our results reveal that the time-bandwidth and Q-factor limits characterizing the storage capacity of (passive, linear) guiding and resonant systems in physics and engineering are not as "fundamental" as has conventionally been thought and can be broken to an arbitrarily large degree, so long as Lorentz reciprocity is broken in those systems. To this end, further means of breaking unidirectionality (*22*), such as parity-time–symmetry media (*31*) or topological insulators (*32*–*34*), might also be of interest. We believe that it is now possible to design ultrahigh-Q resonant systems in atomic, optical, and condensed matter physics, as well as in mechanical and electrical engineering, with unprecedentedly high bandwidths and ultrafast response times, in addition to ultraslow- and stopped-light systems with unusually high delay-bandwidth products, for a wide range of applications in those fields (*3*, *8*–*10*, *16*–*18*, *23*, *24*).

REFERENCES AND NOTES

1. E. I. Green, *Am. Sci.* **43**, 584–594 (1955).
2. K. S. Johnson, *Transmission Circuits for Telephonic Communication* (Western Electric, 1924).
3. A. E. Siegman, *Lasers* (Univ. Science Books, Sausalito, CA, 1986), pp. 105–108.
4. K. J. Vahala, *Nature* **424**, 839–846 (2003).
5. W. Ketterle, 8.421 Atomic and Optical Physics I, Spring 2014 (Massachusetts Institute of Technology: MIT OpenCourseWare, 2014), min. 1:09:00; http://ocw.mit.edu/8-421S14.
6. A. Papoulis, *Signal Analysis* (McGraw-Hill, 1977), sect. 8.2.
7. R. W. Boyd, D. J. Gauthier, A. L. Gaeta, A. E. Willner, *Phys. Rev. A* **71**, 023801 (2005).
8. P. W. Milonni, *Fast Light, Slow Light, and Left-Handed Light* (Institute of Physics Series in Optics and Optoelectronics, CRC Press, 2005).
9. J. B. Khurgin, R. S. Tucker Eds., *Slow Light: Science and Applications* (CRC Press, 2009).
10. R. W. Boyd, D. J. Gauthier, *Science* **326**, 1074–1077 (2009).
11. L. V. Hau, S. E. Harris, Z. Dutton, C. H. Behroozi, *Nature* **397**, 594–598 (1999).
12. M. D. Lukin, A. Imamoğlu, *Nature* **413**, 273–276 (2001).
13. D. A. B. Miller, *Phys. Rev. Lett.* **99**, 203903 (2007).
14. J. B. Khurgin, *Adv. Opt. Photonics* **2**, 287–318 (2010).
15. Q. Xu, P. Dong, M. Lipson, *Nat. Phys.* **3**, 406–410 (2007).
16. L. Novotny, B. Hecht, *Principles of Nano-Optics* (Cambridge Univ. Press, 2012).
17. H. A. Haus, *Waves and Fields in Optoelectronics* (Prentice-Hall, 1984), chap. 7.
18. K. Vahala, *Optical Microcavities* (World Scientific, 2005).
19. See supplementary materials.
20. J. J. Brion, R. F. Wallis, A. Hartstein, E. Burstein, *Phys. Rev. Lett.* **28**, 1455–1458 (1972).
21. L. Shen, Y. You, Z. Wang, X. Deng, *Opt. Express* **23**, 950–962 (2015).
22. D. Jalas *et al.*, *Nat. Photonics* **7**, 579–582 (2013).
23. D. M. Pozar, *Microwave Engineering* (Wiley, 2011).
24. S. M. Dutra, *Cavity Quantum Electrodynamics: The Strange Theory of Light in a Box* (Wiley, 2005), p. 34.
25. R. Zhang, S. R. Garner, L. V. Hau, *Phys. Rev. Lett.* **103**, 233602 (2009).
26. J. Gómez Rivas, C. Janke, P. Bolivar, H. Kurz, *Opt. Express* **13**, 847–859 (2005).
27. R. W. Boyd, *J. Opt. Soc. Am. B* **28**, A38–A44 (2011).
28. W. H. Wee, J. B. Pendry, *Phys. Rev. Lett.* **106**, 165503 (2011).
29. U. Leonhardt, T. Tyc, *Science* **323**, 110–112 (2009).
30. F. Monticone, A. Alù, *Optica* **3**, 718–724 (2016).
31. C. E. Rüter *et al.*, *Nat. Phys.* **6**, 192–195 (2010).
32. M. Z. Hasan, C. L. Kane, *Rev. Mod. Phys.* **82**, 3045–3067 (2010).
33. M. C. Rechtsman *et al.*, *Nature* **496**, 196–200 (2013).
34. A. B. Khanikaev *et al.*, *Nat. Mater.* **12**, 233–239 (2013).

ACKNOWLEDGMENTS

K.L.T. gratefully acknowledges the support of the Eugen Lommel fellowship of the Max Planck Institute for the Science of Light (Erlangen) and R.W.B. the Canada Excellence Research Chairs Program. H.A. and K.L.T. supported by European Commission Horizon 2020 (grant no. FETOPEN-737071), ULTRA-CHIRAL Project. L.S. supported by National Natural Science Foundation of China grant no. 61372005 and key project grant no. 41331070.

SUPPLEMENTARY MATERIALS

www.sciencemag.org/content/356/6344/1260/suppl/DC1
Materials and Methods
Figs. S1 to S3
Table S1
References

23 December 2016; accepted 25 May 2017
10.1126/science.aam6662

Science

Breaking Lorentz reciprocity to overcome the time-bandwidth limit in physics and engineering

K. L. Tsakmakidis, L. Shen, S. A. Schulz, X. Zheng, J. Upham, X. Deng, H. Altug, A. F. Vakakis and R. W. Boyd

Science **356** (6344), 1260-1264.
DOI: 10.1126/science.aam6662

Resonant systems with high bandwidth

The performance of an active system, whether it is optical, electrical, or mechanical, is often described by its quality (*Q*) factor. Typically, one learns the rule that the higher the *Q* factor, the sharper the resonance —that is, the bandwidth of the device is reduced. Tsakmakidis *et al.* show that this is indeed the case, but only for symmetric systems. However, for the case of asymmetric (or nonreciprocal) systems, the rule need not be obeyed. They show theoretically that the more asymmetric a system with high *Q* is, the wider the bandwidth can be. The effect raises the prospect of designing high- *Q* devices operating over large bandwidths.

Science, this issue p. 1260

www.sciencemag.org/content/356/6344/1260/suppl/DC1

Supplementary Materials for

Breaking Lorentz reciprocity to overcome the time-bandwidth limit in physics and engineering

K. L. Tsakmakidis,* L. Shen, S. A. Schulz, X. Zheng, J. Upham, X. Deng, H. Altug, A. F. Vakakis, R. W. Boyd*

*Corresponding author. Email: kostsakmakidis@gmail.com (K.L.T.); rboyd@uottawa.ca (R.W.B.)

Published 23 June 2017, *Science* **356**, 1260 (2017)
DOI: 10.1126/science.aam6662

This PDF file includes:

Materials and Methods
Figs. S1 to S3
Table S1
References

Materials and Methods

Bandwidth and lifetime characteristics of reciprocal and non-reciprocal devices

There are subtle but important differences between the (bandwidth, lifetime and Q-factor) characteristics of reciprocal and non-reciprocal devices, thus appropriate care should accordingly be exercised when analyzing the above characteristics of such devices.

Specifically, as shown in the first row of Table S1 below, the key property in a reciprocal device is that because of time-reversal invariance the rates of input and output of energy into/from the device are equal (*17*, *18*), $\rho_{in} = 2/\tau_{in} = \rho_{out} = 2/\tau_{out}$, where the factor of '2' arises because ρ_{in} and ρ_{out} refer to the energy (rather than the amplitude) rate (*17*). Furthermore, we normally operate in the underdamped regime, where energy can couple into the device before it dissipates, i.e.

$$2/\tau_{in} = 2/\tau_{out} >> 2/\tau_0 \rightarrow \rho_{in} = \rho_{out} >> 2/\tau_0 \qquad \text{(S1)}$$

with $2/\tau_0$ being the energy-decay rate owing to internal, dissipative/Joule losses. With these notes in mind, we may use the well-known expression for the 'loaded in-coupling Q', $Q_{L,in}$ (*17*), summarized in the last raw of Table S1 (Eq. (S3)), to calculate an approximate relation linking the in-coupling bandwidth $\Delta\omega_{in}$ (i.e., the bandwidth available at the input port of the device) to the in-coupling rate ρ_{in}:

$$\frac{1}{Q_{L,in}} = \frac{\Delta\omega_{in}}{\omega_0} \xrightarrow{\text{(S3)}} = \frac{2\pi/\tau_0}{\omega_0} + \frac{\pi\rho_{in}}{\omega_0} \xrightarrow{\text{(S1)}} \boxed{\Delta\omega_{in} \approx \pi\rho_{in}}. \qquad \text{(S2)}$$

Reciprocal	Non-reciprocal
One bandwidth ($\Delta\omega_{in} = \Delta\omega_{out} = \Delta\omega$) $\Delta\omega_{in} = \pi\rho_{in}$ $\Delta\omega_{out} = \boxed{\pi\rho_{out} = \pi\rho_{in}} = \Delta\omega_{in}$	**Two** bandwidths ($\Delta\omega_{in} \neq \Delta\omega_{out}$) $\Delta\omega_{in} = \pi\rho_{in} >> \pi\rho_{out} = \Delta\omega_{out}$ $\Delta\omega_{out} = 2\pi/\tau_0$ ($\rho_{out} \rightarrow 0 \Rightarrow \tau_{out} \rightarrow \infty$)
$\Delta\tau = \tau_{out} = \frac{2}{\rho_{out}} = \frac{2}{\rho_{in}} = \frac{2\pi}{\Delta\omega}$	$\Delta\tau = \tau_0 \neq \frac{2}{\rho_{in}} = \frac{2\pi}{\Delta\omega_{in}}$
$\frac{1}{Q_{L,in}} = \frac{1}{Q_0} + \frac{1}{Q_{in}}$ (S3)	$\frac{1}{Q_{L,in}} = \frac{1}{Q_0} + \frac{1}{Q_{in}}$ $\frac{1}{Q_{L,out}} = \frac{1}{Q_0} + \frac{1}{Q_{out}}$

Table S1. Bandwidth, lifetime and Q-factor characteristics of reciprocal and non-reciprocal resonant devices.

The situation is drastically different in highly asymmetric, non-reciprocal devices where the in-coupling rate may be much larger than the out-coupling rate, $\rho_{in} >> \rho_{out}$. In such a device, while the in-coupling bandwidth $\Delta\omega_{in}$ is still proportional to the in-coupling rate, $\Delta\omega_{in} \propto \rho_{in}$, and can therefore be large, the out-coupling bandwidth $\Delta\omega_{out}$ is proportional to the out-coupling rate, $\Delta\omega_{out} \propto \rho_{out}$, and for large asymmetry (as in the herein considered structure, in which the in-coupling rate is large but nothing can escape from the localization point at the rightmost end; see Fig. 2B) it can become zero, $\Delta\omega_{out} \rightarrow 0$ ($\Rightarrow \tau_{out} \rightarrow \infty$). Thus, in that case, the lifetime of the excitation $\Delta\tau = 1/(1/\tau_0 + 1/\tau_{out})$ now

becomes equal to τ_0 ($\Delta\tau \approx \tau_0$), as shown in the second row of Table S1 above, rather than equal to τ_{out} as was the case for (the underdamped regime of) reciprocal devices. Importantly, in that case, the lifetime $\Delta\tau$ (being equal to τ_0) is completely decoupled from the in-coupling rate and bandwidth, i.e. $\Delta\tau \neq 2/\rho_{in} = 2\pi/\Delta\omega_{in}$, simply because time-reversal symmetry linking ρ_{in} to ρ_{out} (see highlighted box in the first row of Table S1) is not valid anymore (as the system is non-reciprocal, i.e. Lorentz reciprocity is broken, e.g. by application of an external magnetic bias as in the heterostructure of Fig. 2B). By contrast, as inferred from the above discussion and as summarized in the left column of Table S1, for reciprocal devices it is always $\Delta\tau = 2\pi/\Delta\omega_{in}$, and hence the time-bandwidth product is always constant – or, generally, upper-limited. Since time invariance does not apply anymore in devices where Lorentz reciprocity is broken, and $\Delta\tau \neq 2\pi/\Delta\omega_{in}$, the time-bandwidth product may, now, in principle, take-on arbitrarily large values – much higher that what was, until now, considered to be the 'fundamental' upper limit characterizing reciprocal resonant and waveguiding systems (which, as explained in the main text, is usually thought to 'fundamentally' arise from basic Fourier-transform considerations in the derivation of the frequency response of lossy resonators and guiding systems (*1-5*, *7*, *9*, *13-18*)).

Parameters used in results/figures shown in the main text

In the attaining the band diagram of **Fig. 2C**, the following optogeometric parameters were used:

– Magnetized InSb: $N_e = 1.1\times10^{16}$ cm^{-3} (electron density) (*23*, *26*); $\varepsilon_\infty = 15.6$; $\omega_p = [(N_e e^2)/(\varepsilon_\infty\varepsilon_0 m^*)]^{1/2} = 4\pi\times10^{12}$ rad/s (effective plasma frequency); $f_p = \omega_p/2\pi = 2$ THz; $B_0 = 0.2$ T (external magnetic field); $\omega_c = eB_0/m^* = 0.2\omega_p$ (electron cyclotron frequency).

– Si layer: $\varepsilon_r = 11.68$; $d = 0.08\lambda_p = 12$ μm ($\lambda_p = c/f_p = 150$ μm).

– Ag metal: $\varepsilon_{Ag} = 1 - \omega_{pe}^2/[\omega(\omega + i\omega_\tau)]$, with $\omega_{pe} = 1.367\times10^{16}$ rad/s and $\omega_\tau = 2.733 \times 10^{13}$ rad/s.

For the simulation results of **Fig. 3**, the following parameters were used:

– Waveguide length: $L = 800$ μm; loss of InSb: $v = 0.001\omega_p$.

– Magnetic current line source: $I_m(t) = \exp[-(t - t_0)^2/\tau^2]\exp(-i2\pi f_0 t)$, where $f_0 = 1.5$ THz, $t_0 = 15T_p$; $\tau = 6.4T_p$ (with $T_p = 2\pi/\omega_p = 0.5$ ps), positioned 100 μm away from the leftmost end and 6 μm above the Si/InSb interface. The spectrum of the source is $A(\omega) = A_0\exp[-(f-f_0)^2/\Delta f^2]$, with $\Delta f = 0.1$ THz (FWHM = 0.1665 THz).

For the simulation results of **Figs. 4A, B** (where v was variable) the used optogeometric parameters were the same as those used in Figs. 2 and 3, but with $t_0 = 80T_p$, $\tau = 31.8T_p$ and $\Delta f = 0.02$ THz.

For the simulation results of **Figs. 4C, D** (where ω_c or B_0 were variable) the used optogeometric parameters were the same as those used in Figs. 2, 3, 4A, 4B.

Dispersion relation (Eq. (6)) and FDTD simulations

To obtain the dispersion equation (Eq. (6)) in the main body of the paper, we assume that the excited surface magnetoplasmon (SMP) in the heterostructure of Fig. 2B is transverse magnetic (TM, or *p*-) polarized, with the nonzero component of the magnetic field, H_y, having the following spatio-temporal variation:

$H_y(x, z) = [A_1\exp(-\alpha_d x) + A_2\exp(\alpha_d x)]\exp[i(kz - \omega t)]$, in the Si layer ($0 \le x \le d$),

$H_y(x, z) = B\exp(\alpha_s x)\exp[i(kz - \omega t)]$, in the semiconductor/InSb layer ($x \le 0$),

and $H_y(x, z) = C\exp(-\alpha_m x)\exp[i(kz - \omega t)]$, in the upper metal/Ag ($x \ge 0$),

where k is the longitudinal propagation constant, and the remaining parameters are defined in the main text. The E_z component can be obtained from the above expressions for H_y as: $E_z = [i/(\omega\varepsilon)]\,\partial H_y/\partial x$. Upon matching the two tangential field components at the Si/InSb and Ag/Si interfaces we immediately obtain the transcendental dispersion relation, Eq. (6), in the main text of the paper.

For the full-wave simulation results shown in Figs. 3 and 4 in the main text (and in Fig. S1 below), we used the finite-difference time-domain (FDTD) method. The relevant equations in the gyroelectric semiconductor (InSb) are then:

$$\frac{\partial E_y}{\partial x} - \frac{\partial E_x}{\partial y} = -\mu_0 \frac{\partial H_z}{\partial t},$$

$$\frac{\partial H_z}{\partial y} = \varepsilon_0\varepsilon_\infty \frac{\partial E_x}{\partial t} + (J_x^- + J_x^+) + i(J_y^- - J_y^+),$$

$$-\frac{\partial H_z}{\partial x} = \varepsilon_0\varepsilon_\infty \frac{\partial E_y}{\partial t} - i(J_x^- - J_x^+) + i(J_y^- + J_y^+),$$

$$\frac{\partial J_{x,y}^{\pm}}{\partial t} + (\nu \mp i\omega_c)J_{x,y}^{\pm} = \frac{1}{2}\varepsilon_0\omega_p^2 E_{x,y}. \qquad \text{(S4a-d)}$$

The magnetic current line source was of the form: $I_m = \exp[-(t-t_0)^2/\tau^2]\exp(-i2\pi f_0 t)$, $t \ge 0$, and was exciting a pulse whose bandwidth was in all cases within the 'complete unidirectional propagation' (CUP) region of the band-diagram (Fig. 2C). Figures S1(A)-(E) below illustrate successive snapshots from these time-domain simulations:

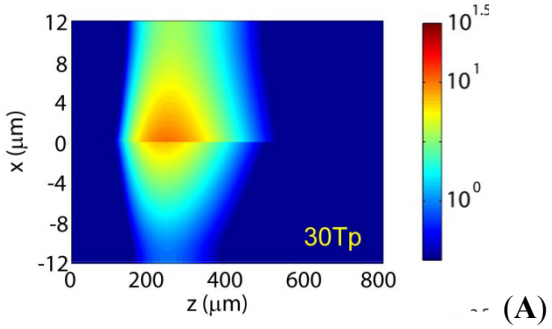

(A)

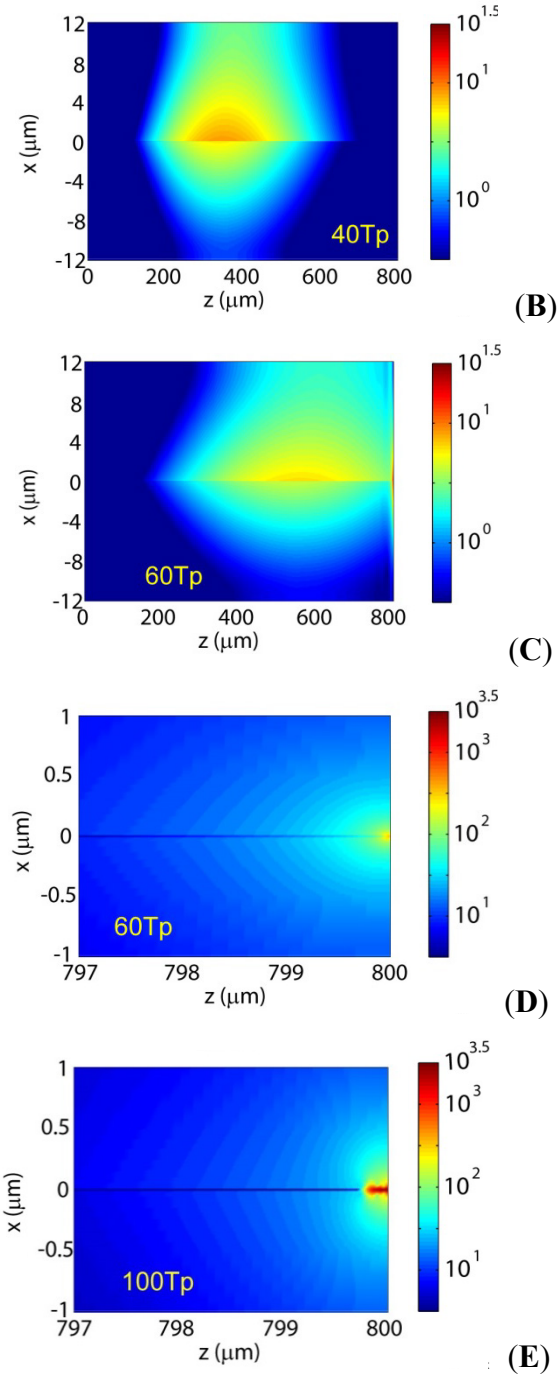

Figure S1. Propagation and trapping dynamics. Successive snapshots of the propagation of a surface magnetoplasmon along the gyroelectric semiconductor heterostructure of Fig. 2B, with its eventual localization (and thereafter absorption; not shown here) at the rightmost end. Shown here are the successive distributions of the **E**-field amplitude. Note the change of scale in the colorbar and in the horizontal axis in parts D and E, as compared with parts A-C.

In the FDTD simulations we used a uniform grid mesh with Δx = 0.1 μm and Δz = 0.5 μm, apart from the region close to the Si/InSb interface and the rightmost Si-InSb/Ag interfaces where a non-uniform mesh was used with δx = 1/128 μm and δz = 1/512 μm

(otherwise, non-convergence or spurious back-reflections may be observed). Also, for the results of Fig. 3B we used a computational box of side length 4 μm, located around the rightmost Si-InSb/Ag interfaces, to record the time evolution of the electromagnetic energy inside it (where, e.g., the energy density inside the dispersive semiconductor is given by $U_s = (1/4)\mathbf{E}^* \mathrm{d}(\omega\vec{\varepsilon}_{\mathrm{InSb}})/\mathrm{d}\omega\mathbf{E} + (1/4)\mu_0 |\mathbf{H}|^2$).

Derivation of Eq. (1) in the main text

Let us assume that the field amplitude α inside a resonant system varies with time as $\alpha(t) \propto \cos(\omega_0 t)\mathrm{e}^{-(1/2)\Gamma t}$, for $t \geq 0$. The Fourier transform of this expression reads: $A(\omega) = (\Gamma/2 + i\omega)/[(\Gamma/2 + i\omega)^2 + \omega_0^2]$. In the resonance approximation, we have (*3*): $\omega_0^2 - \omega^2 = (\omega_0 + \omega)(\omega_0 - \omega) \approx 2\omega_0(\omega_0 - \omega) \approx 2\omega(\omega_0 - \omega)$. Furthermore, in the underdamped regime mentioned above, we assume that $\Gamma/2 << \omega_0$. With these approximations in mind, we successively have for $A(\omega)$:

$$
\begin{aligned}
A(\omega) &= \frac{\Gamma/2 + i\omega_0}{2\omega_0}\frac{1}{\omega_0 - \omega + i\Gamma/2} \\
&= \frac{\omega_0 - i\Gamma/2}{\Gamma\omega_0}\frac{1}{1 - i[(\omega - \omega_0)/\Gamma/2]} \Rightarrow \\
I(\omega) \propto |A(\omega)|^2 &= \frac{\omega_0^2 + (\Gamma/2)^2}{(\Gamma\omega_0)^2}\frac{(\Gamma/2)^2}{(\omega - \omega_0)^2 + (\Gamma/2)^2},
\end{aligned}
\tag{S5}
$$

which is Eq. (1) used in the main text.

Preservation of bandwidth during the static trapping and storage

In this linear, time-invariant system, the "bandwidth" is essentially the in-coupling bandwidth $\Delta\omega_{\mathrm{in}}$ associated with the in-coupling rate ρ_{in}: the higher ρ_{in} becomes, the larger does the stored/trapped bandwidth ($\Delta\omega_{\mathrm{in}}$) become. Therefore, this ($\Delta\omega = \Delta\omega_{\mathrm{in}}$) is the bandwidth that is stored/trapped in our asymmetric resonant system, assuming that $\Delta\omega_{\mathrm{in}}$ lies completely within the CUP region. The out-coupling bandwidth $\Delta\omega_{\mathrm{out}}$ ($\approx 2\pi/\tau_0$) is dependent on the material loss for the herein considered perfectly asymmetric case where $\rho_{\mathrm{out}} \rightarrow 0$. While the loss spectrum can have a sharp resonance (in fact, one is required to achieve a low loss rate) this can be centered on a frequency far from the operating range, with a weak dependence of loss on frequency in the relevant frequency regime – see Fig. S2(C). Thus, in this nonreciprocal system, both, large storage times $\Delta\tau = \tau_0$ (i.e., small out-coupling bandwidths $\Delta\omega_{\mathrm{out}} \approx 2\pi/\tau_0$ lost from the in-coupling bandwidth $\Delta\omega_{\mathrm{in}}$) and large bandwidths ($\Delta\omega = \Delta\omega_{\mathrm{in}}$ large for high ρ_{in}) are simultaneously possible – whereas conventionally, for reciprocal systems, $\Delta\tau$ and $\Delta\omega$ are fundamentally reciprocal to one another.

To more clearly illustrate these, Fig. S2 below summarizes the spectrum of our pulse at various locations (i.e., at various/different time instances) as it is progressively trapped and stored into its trapping region at the terminated, rightmost end of the heterostructure (Fig. S2(A) below). One may clearly see from these results that the whole spectrum of the pulse is rigorously stored in its trapping region in this static, linear system – unlike, e.g., what one might have expected for time-varying or nonlinear resonant systems, in

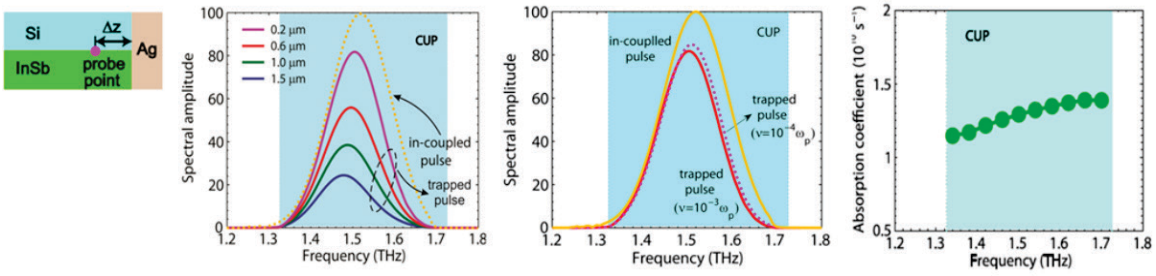

(A) **(B)** **(C)**

Figure S2: Absorption spectra during the resonant storage and during the pulse's propagation. (A) Spectrum of trapped pulse at several points in the trapping region (cf. leftmost panel), and (B) for two different values of InSb loss factor v, at a point $\Delta z = 0.2$ μm (cf. leftmost panel) in both cases shown in (B). (C) Calculated from full-wave simulations optical losses within the 'complete unidirectional propagation' (CUP) band for $v = 0.001\omega_p$.

which case the spectrum would have been manipulated. The small redshift that we observe in the spectra of the stored pulse at various locations (time instances) in Fig. S2(A) is attributed to the slightly increased optical losses with frequency in our structure, as was calculated from full-wave simulations and is shown in Fig. S2(C) above. Likewise, Fig. S2(B) shows that the spectra of the trapped pulse remain unaffected when varying the InSb loss factor v, as expected, since as mentioned above the magnitude of the material losses cannot change the shape of the spectra (such a modification might have been caused, e.g., by a change in the dispersion / 'slope' of the material losses).

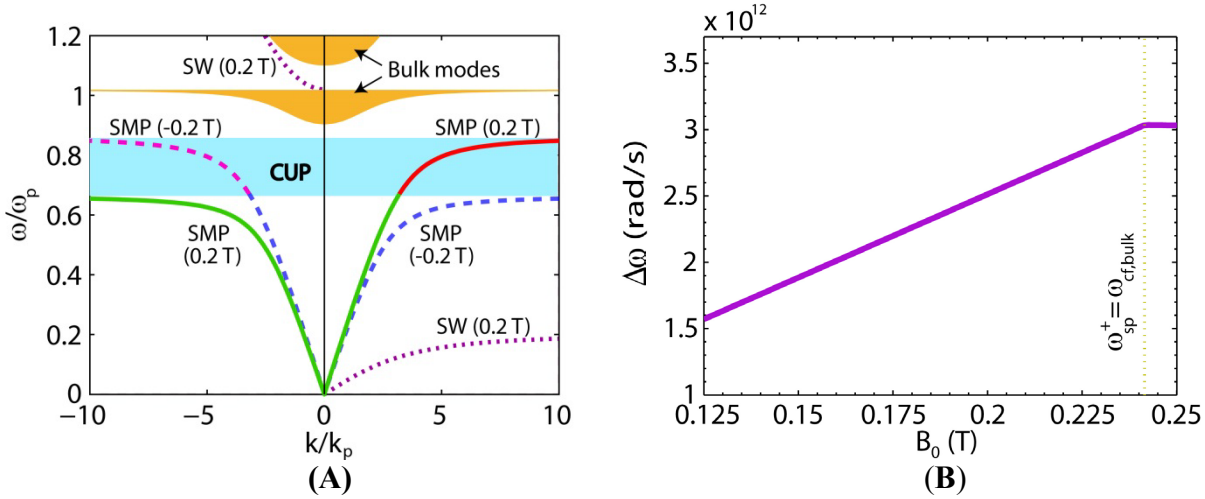

(A) **(B)**

Figure S3. Bandstructure and bandwidth of the unidirectional-propagation region. (A) Band diagram of the heterostructure of Fig. 2B (cf. Fig. 2C), but now also shown is the case where a static magnetic bias $B_0 = 0.2$ T is applied in the $+y$ direction. The curve corresponding to that case is shown with a dashed line. (B) Shown here is the blue solid line of Fig. 4C but now plotted on a linear scale, showing clearly the gradual increase of the structure's bandwidth with increasing magnetic field B_0 (cf. remarks immediately after Eq. (7)).

References and Notes

1. E. I. Green, The story of *Q*. *Am. Sci.* **43**, 584–594 (1955).

2. K. S. Johnson, *Transmission Circuits for Telephonic Communication* (Western Electric, 1924).

3. A. E. Siegman, *Lasers* (Univ. Science Books, Sausalito, CA, 1986), pp. 105–108.

4. K. J. Vahala, Optical microcavities. *Nature* **424**, 839–846 (2003). doi:10.1038/nature01939 Medline

5. W. Ketterle, 8.421 Atomic and Optical Physics I, Spring 2014 (Massachusetts Institute of Technology: MIT OpenCourseWare, 2014), min. 1:09:00; http://ocw.mit.edu/8-421S14.

6. A. Papoulis, *Signal Analysis* (McGraw-Hill, 1977), sect. 8.2.

7. R. W. Boyd, D. J. Gauthier, A. L. Gaeta, A. E. Willner, Maximum time delay achievable on propagation through a slow-light medium. *Phys. Rev. A* **71**, 023801 (2005). doi:10.1103/PhysRevA.71.023801

8. P. W. Milonni, *Fast Light, Slow Light, and Left-Handed Light* (Institute of Physics Series in Optics and Optoelectronics, CRC Press, 2005).

9. J. B. Khurgin, R. S. Tucker Eds., *Slow Light: Science and Applications* (CRC Press, 2009).

10. R. W. Boyd, D. J. Gauthier, Controlling the velocity of light pulses. *Science* **326**, 1074–1077 (2009). doi:10.1126/science.1170885 Medline

11. L. V. Hau, S. E. Harris, Z. Dutton, C. H. Behroozi, Light speed reduction to 17 metres per second in an ultracold atomic gas. *Nature* **397**, 594–598 (1999). doi:10.1038/17561

12. M. D. Lukin, A. Imamoğlu, Controlling photons using electromagnetically induced transparency. *Nature* **413**, 273–276 (2001). doi:10.1038/35095000 Medline

13. D. A. B. Miller, Fundamental limit to linear one-dimensional slow light structures. *Phys. Rev. Lett.* **99**, 203903 (2007). doi:10.1103/PhysRevLett.99.203903 Medline

14. J. B. Khurgin, Slow light in various media: A tutorial. *Adv. Opt. Photonics* **2**, 287–318 (2010). doi:10.1364/AOP.2.000287

15. Q. Xu, P. Dong, M. Lipson, Breaking the delay-bandwidth limit in a photonic structure. *Nat. Phys.* **3**, 406–410 (2007). doi:10.1038/nphys600

16. L. Novotny, B. Hecht, *Principles of Nano-Optics* (Cambridge Univ. Press, 2012).

17. H. A. Haus, *Waves and Fields in Optoelectronics* (Prentice-Hall, 1984), chap. 7.

18. K. Vahala, *Optical Microcavities* (World Scientific, 2005).

19. See supplementary materials.

20. J. J. Brion, R. F. Wallis, A. Hartstein, E. Burstein, Theory of surface magnetoplasmons in semiconductors. *Phys. Rev. Lett.* **28**, 1455–1458 (1972). doi:10.1103/PhysRevLett.28.1455

21. L. Shen, Y. You, Z. Wang, X. Deng, Backscattering-immune one-way surface magnetoplasmons at terahertz frequencies. *Opt. Express* **23**, 950–962 (2015). doi:10.1364/OE.23.000950 Medline

22. D. Jalas, A. Petrov, M. Eich, W. Freude, S. Fan, Z. Yu, R. Baets, M. Popović, A. Melloni, J. D. Joannopoulos, M. Vanwolleghem, C. R. Doerr, H. Renner, What is – and what is not – an optical isolator. *Nat. Photonics* **7**, 579–582 (2013). doi:10.1038/nphoton.2013.185

23. D. M. Pozar, *Microwave Engineering* (Wiley, 2011).

24. S. M. Dutra, *Cavity Quantum Electrodynamics: The Strange Theory of Light in a Box* (Wiley, 2005), p. 34.

25. R. Zhang, S. R. Garner, L. V. Hau, Creation of long-term coherent optical memory via controlled nonlinear interactions in Bose-Einstein condensates. *Phys. Rev. Lett.* **103**, 233602 (2009). doi:10.1103/PhysRevLett.103.233602 Medline

26. J. Gómez Rivas, C. Janke, P. Bolivar, H. Kurz, Transmission of THz radiation through InSb gratings of subwavelength apertures. *Opt. Express* **13**, 847–859 (2005). doi:10.1364/OPEX.13.000847 Medline

27. R. W. Boyd, Material slow light and structural slow light: Similarities and differences for nonlinear optics. *J. Opt. Soc. Am. B* **28**, A38–A44 (2011). doi:10.1364/JOSAB.28.000A38

28. W. H. Wee, J. B. Pendry, Universal evolution of perfect lenses. *Phys. Rev. Lett.* **106**, 165503 (2011). doi:10.1103/PhysRevLett.106.165503 Medline

29. U. Leonhardt, T. Tyc, Broadband invisibility by non-Euclidean cloaking. *Science* **323**, 110–112 (2009). doi:10.1126/science.1166332 Medline

30. F. Monticone, A. Alù, Invisibility exposed: Physical bounds on passive cloaking. *Optica* **3**, 718–724 (2016). doi:10.1364/OPTICA.3.000718

31. C. E. Rüter, K. G. Makris, R. El-Ganainy, D. N. Christodoulides, M. Segev, D. Kip, Observation of parity-time symmetry in optics. *Nat. Phys.* **6**, 192–195 (2010). doi:10.1038/nphys1515

32. M. Z. Hasan, C. L. Kane, *Colloquium*: Topological insulators. *Rev. Mod. Phys.* **82**, 3045–3067 (2010). doi:10.1103/RevModPhys.82.3045

33. M. C. Rechtsman, J. M. Zeuner, Y. Plotnik, Y. Lumer, D. Podolsky, F. Dreisow, S. Nolte, M. Segev, A. Szameit, Photonic Floquet topological insulators. *Nature* **496**, 196–200 (2013). doi:10.1038/nature12066 Medline

34. A. B. Khanikaev, S. H. Mousavi, W.-K. Tse, M. Kargarian, A. H. MacDonald, G. Shvets, Photonic topological insulators. *Nat. Mater.* **12**, 233–239 (2013). doi:10.1038/nmat3520 Medline